Ion Acoustic Waves and Related Plasma Observations in the Solar Wind

D. A. GURNETT

Department of Physics and Astronomy, The University of Iowa, Iowa City, Iowa 52242

E. MARSCH, W. PILIPP, AND R. SCHWENN

Max-Planck-Institut für Physik und Astrophysik, Institut für extraterrestrische Physik 8046 Garching, West Germany

H. ROSENBAUER

Max-Planck-Institut für Aeronomie, 3411 Katlenburg-Lindau 3, West Germany

This paper presents an investigation of solar wind ion acoustic waves and their relationship to the macroscopic and microscopic characteristics of the solar wind plasma. Comparisons with the overall solar wind corotational structure show that the most intense ion acoustic waves usually occur in the low-velocity regions ahead of high-speed solar wind streams. Of the detailed plasma parameters investigated, the ion acoustic wave intensities are found to be most closely correlated with the electron to proton temperature ratio T_e/T_p and with the electron heat flux. Investigations of the detailed electron and proton distribution functions also show that the ion acoustic waves usually occur in regions with highly non-Maxwellian distributions characteristic of double-proton streams. The distribution functions for the double-proton streams are usually not resolved into two clearly defined peaks, but rather they appear as a broad shoulder on the main proton distribution. Two main mechanisms, an electron heat flux instability and a double-ion beam instability, are considered for generating the ion-acoustic-like waves observed in the solar wind. Both mechanisms have favorable and unfavorable features. The electron heat flux mechanism can account for the observed waves at moderate to large ratios of T_e/T_p but has problems when T_e/T_p is small, as sometimes occurs. The ion beam instability appears to provide more flexibility in the T_e/T_p ratio; however, detailed comparisons using observed distribution functions indicate that the ion beam mode is usually stable. Possible resolutions of these difficulties are discussed.

1. INTRODUCTION

Plasma wave observations on the Helios and Voyager spacecraft [*Gurnett and Anderson*, 1977; *Gurnett and Frank*, 1978; *Kurth et al.*, 1979] have demonstrated that short-wavelength electrostatic waves are frequently present in the solar wind at frequencies between the ion and electron plasma frequencies, $f_p^+ < f < f_p^-$. The primary characteristics of these waves are that they occur in brief monochromatic bursts with a rapidly varying center frequency. The frequency spectrum of these bursts varies systematically with radial distance from the sun, as is illustrated in Figure 1, decreasing in frequency with increasing radial distance. The upper and lower frequency limits of the spectrum are approximately f_p^+ and f_p^-. The electric field of the waves tends to be aligned along the direction of the solar wind magnetic field, within approximately 15° or less. The waves tend to occur in distinct 'storms' lasting from a few hours to several days, separated by intervals of a few days during which little or no activity is detected.

Only three types of plasma wave modes are known which can account for the characteristics of the electrostatic waves detected by Helios and Voyager. These modes are the Buneman mode [*Buneman*, 1958] at $f_B \simeq (m^-/m^+)^{1/3} f_p^-$, the ion acoustic mode at $f \lesssim f_p^+$, and electron plasma oscillations at $f \simeq f_p^-$. Both the ion acoustic mode and the electron plasma oscillations require large Doppler shifts to explain the observed frequency spectrum. At the present time the existing evidence suggests that short-wavelength ion acoustic waves, Doppler shifted to frequencies $f_p^+ < f < f_p^-$, provide the most likely explanation for the waves detected by Helios and Voyager. This identification is based on the wavelength measurements of *Gurnett and Frank* [1978], who showed that the observed wavelengths provide the correct Doppler shift to account for the observed frequency spectrum. In this case the fact that the frequency spectrum falls in the range $f_p^+ < f < f_p^-$ is purely coincidental, since the overall proportionality to f_p^+ and f_p^- can be explained in terms of the density dependence of the Debye length λ_D, which determines the minimum wavelength and the maximum Doppler shift. Electron plasma oscillations, Doppler shifted downward in frequency, are not considered a very likely possibility for explaining these waves, since such oscillations could only be excited by relatively energetic particles streaming back toward the sun, which have not been observed. Similarly, the Buneman mode is not considered a very likely possibility because of the very large relative drift velocities, and hence currents, which are required to drive this instability. Although a complete understanding of the instability mechanism and mode of propagation has not yet been achieved, we will continue to refer to these waves as ion acoustic waves, following our previous terminology.

The primary objective of this paper is to present a study of the relationship between the interplanetary ion acoustic waves detected by Helios and the macroscopic and microscopic characteristics of the solar wind plasma. For details of the Helios 1 and 2 plasma wave and plasma instruments used in this study, see *Gurnett and Anderson* [1977], *Schwenn et al.* [1975], and *Rosenbauer et al.* [1977]. Special emphasis is placed on determining which plasma parameters play the primary role in controlling the intensity and occurrence of ion acoustic waves in the solar wind. Because it is well known that the ion acoustic instability is very sensitive to the electron to ion temperature ratio [*Stix*, 1962], special attention is given to this parameter. The detailed electron and proton velocity distribution func-

Copyright © 1979 by the American Geophysical Union.

Paper number 9A0110.
0148-0227/79/009A-0110$01.00

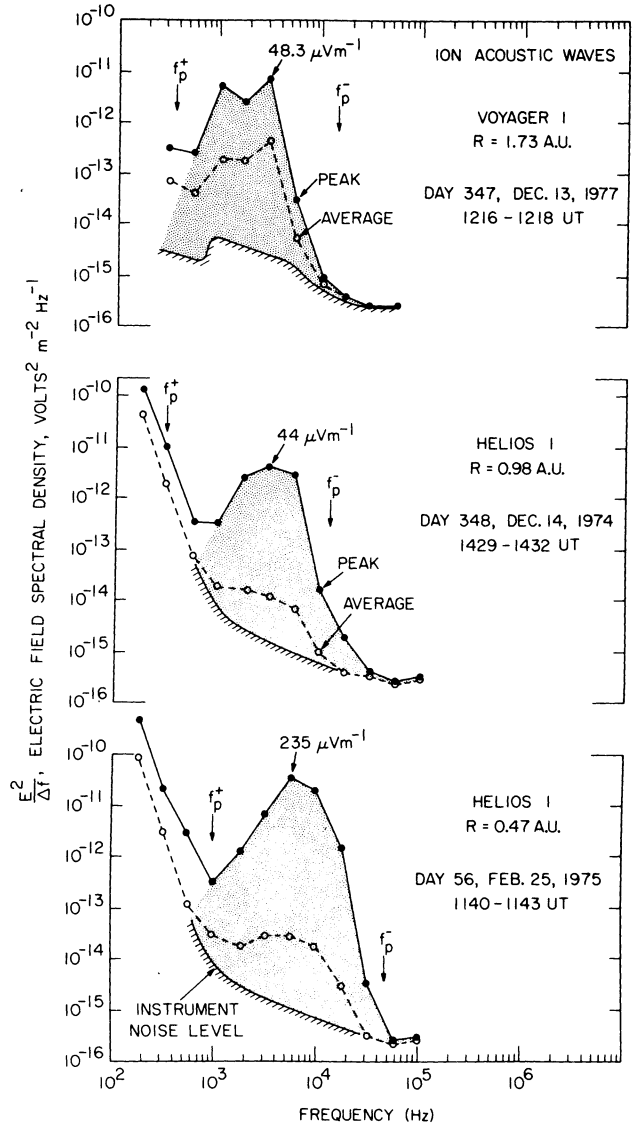

Fig. 1. A series of spectra of the interplanetary ion acoustic waves detected by Helios and Voyager at progressively closer distances to the sun (from top to bottom). The increase in the intensity and the frequency of these waves with decreasing radial distance from the sun is clearly evident.

tions are also examined to try to establish the source of free energy which drives the ion acoustic waves. Both the electron heat flux mechanism of *Forslund* [1970] and the double-ion beam mechanism of *Gary* [1978*a*] are considered.

2. Relationship to Solar Wind Stream Structure

To investigate the relationship between periods of enhanced ion acoustic wave activity and the large-scale corotational structure of the solar wind, a series of combined plots of the plasma wave and plasma data have been made for each solar rotation during the Helios 1 and 2 mission. Three representative plots of this type are shown in Figures 2, 3, and 4. Each plot shows one complete solar rotation. The abscissa is the Carrington longitude of the spacecraft. The day number and heliocentric radial distance are also shown for reference at the bottom of each plot. The top panels give the proton flow speed V_p, density n_p, and temperature T_p as obtained from the Max-Planck plasma instrument. The middle panels give the electric field intensities from the University of Iowa plasma wave instrument in 11 frequency channels extending from 311 Hz to 100 kHz. The solid line in each channel gives the peak electric field intensity, and the vertical bars (black areas) give the average electric field intensity. The dynamic range for each channel is 100 dB, extending from about 10^{-6} to 10^{-1} V m^{-1}. The bottom panels give the electron heat flux Q_e (in units of ergs cm^{-2} s^{-1}) and the electron to proton temperature ratio T_e/T_p.

Two types of waves can be identified in the electric field measurements of Figures 2, 3, and 4: (1) ion acoustic waves in the frequency range from about 1 to 10 kHz and (2) narrow band electron plasma oscillations in the frequency range from about 31.1 to 56.2 kHz. Both the ion acoustic waves and the electron plasma oscillations vary considerably during a solar rotation. Usually, two or three periods of enhanced ion acoustic wave activity occur during each solar rotation, separated by periods of relatively low intensity. The periods of enhanced ion acoustic wave activity usually last from a few hours to several days and are most pronounced in the peak intensity measurements. It should be noted that the peak intensity measurements, which are computed over time intervals of 36.0 min, are extremely sensitive to even very low levels of activity, since even a single burst of noise with a duration greater than 50 ms during any 36.0-min sampling interval will be indicated. Even

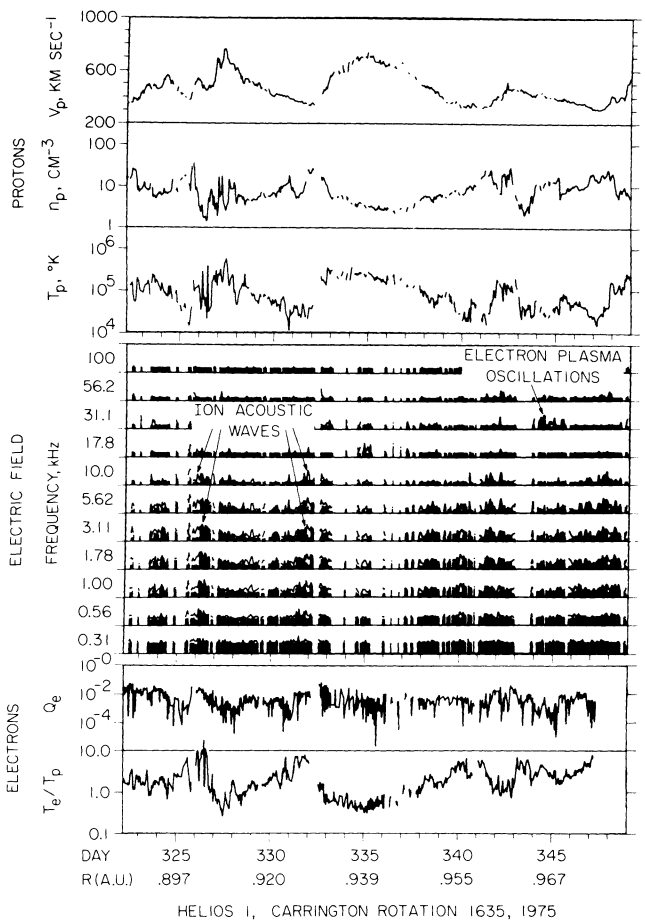

Fig. 2. The plasma wave electric field intensities and solar wind electron and proton parameters for one complete solar rotation, plotted as a function of the Carrington longitude of the spacecraft. Some sproadic ion acoustic wave activity is present nearly all of the time. However, the most intense ion acoustic waves tend to occur in the low-velocity regions ahead of high-speed streams, where T_e/T_p is large, and in regions of large electron heat flux Q_e.

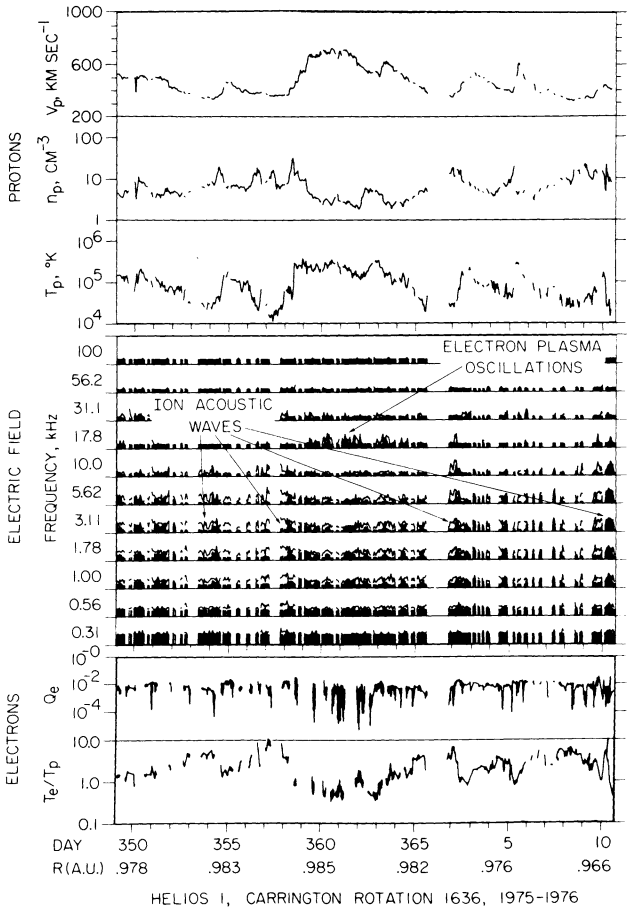

Fig. 3. The plasma wave and solar wind plasma data for the next solar rotation following that of Figure 2. The same general trend, toward large ion acoustic wave intensities ahead of high-speed streams and in regions of large T_e/T_p and Q_e, is again evident.

during quiet periods a low level of ion acoustic wave activity can usually be detected with peak intensities of about 1–10 μV m^{-1}. During more active periods, such as those on day 326 in Figure 2 and days 71–75 in Figure 4, the peak intensities in a given channel (~10% bandwidth) are typically 50–200 μV m^{-1}. The peak intensities are always much larger than the average intensities. The large ratio of peak to average field strengths indicates that the ion acoustic waves consist of many impulsive bursts, with a time interval between the bursts which is much larger than the duration of the bursts.

When the ion acoustic wave intensities are compared with the solar wind velocity measurements, a fairly consistent pattern can be identified in Figures 2, 3, and 4. Whenever a well-defined high-speed stream onset is evident in the proton flow speed V_p, this onset is usually preceded by a period of enhanced ion acoustic wave activity ahead of the high-speed stream. Examples of this relationship can be seen for the high-speed stream onsets on days 327 and 333 in Figure 2, days 357 and 2 in Figure 3, and days 74 and 84 in Figure 4. The ion acoustic waves therefore tend to occur in the low-speed region immediately preceding a high-speed stream interface. Within the high-speed stream regions, where the velocities are greater than about 500 km s^{-1}, the ion acoustic wave intensities are usually quite low. The relationship between the ion acoustic wave intensities and the high- and low-speed stream regions can be placed on a more quantitative basis by computing the average of the 36.0-min peak electric field intensities as a function of the proton flow speed using all of the available data, which include approximately 4 years of observations. The result of this correlation analysis is illustrated in Figure 5, which shows the electric field intensities at 5.62 kHz, roughly in the center of the ion acoustic wave spectrum, averaged in a sequence of contiguous solar wind velocity windows. A negative correlation is clearly evident between the ion acoustic wave intensities and the solar wind velocity, showing that on the average the wave intensities are large in the low-speed solar wind regions. Although Figure 5 indicates a definite negative correlation, a large amount of scatter is also present which tends to reduce the correlation in comparison with what one would expect on the basis of a visual examination of Figures 2, 3, and 4. This scatter usually results from periods, such as the period from day 86 to day 92 in Figure 4, that have a complex structure not simply resolved into low- and high-speed streams.

A more detailed illustration of the electrostatic wave activity observed near a high-speed stream interface is shown on an expanded time scale in Figure 6. This example is for the high-speed stream interface in Figure 4 at about 0940 UT on day 74, 1976. The interface in this case is characterized by a clearly defined tangential discontinuity [*Gosling et al.*, 1978] showing an abrupt increase in the proton flow speed and temperature and a corresponding decrease in the plasma density, which maintains an approximate pressure balance, across the interface. The region of high plasma density, characteristic of the

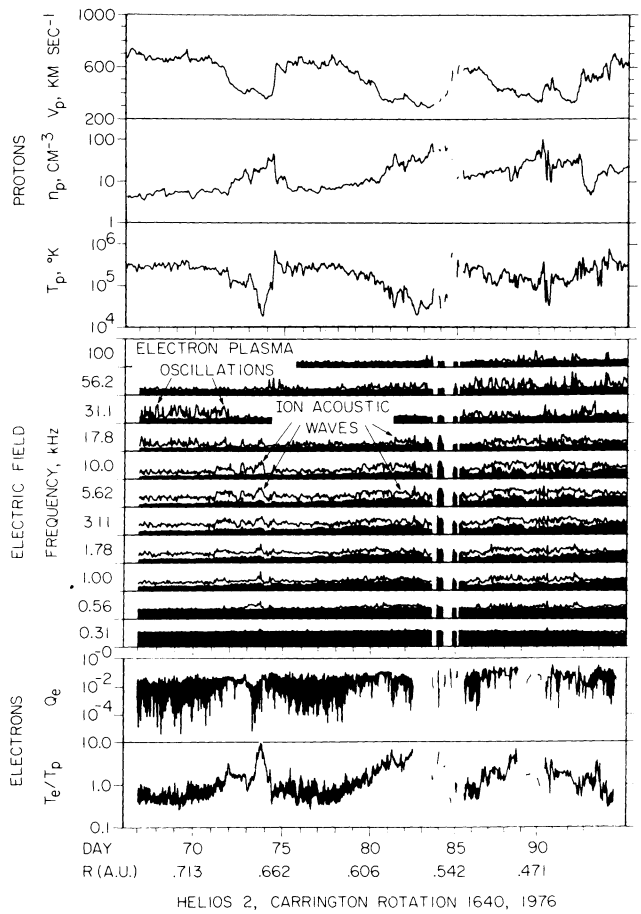

Fig. 4. The plasma wave and solar wind plasma data for another solar rotation similar to Figures 2 and 3. The ion acoustic wave intensities associated with the high-speed stream onset on days 73 and 74 are shown in greater detail in Figure 6.

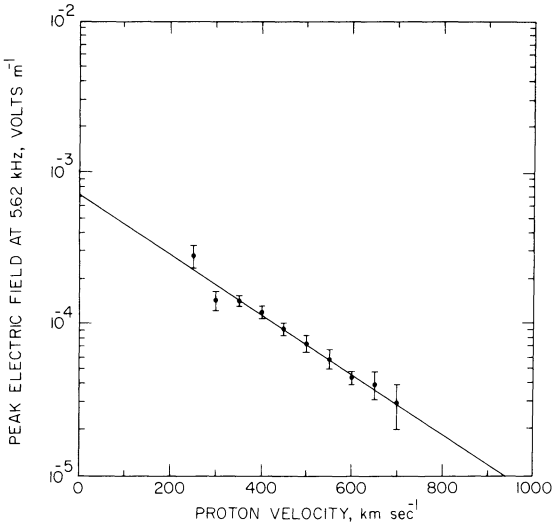

Fig. 5. A plot of the average of the peak 36-min electric field intensities at 5.62 kHz as a function of the solar wind velocity using all of the available Helios 1 and 2 data. The error bars are the standard deviation of the average solar wind velocity in each interval. This illustration shows the general trend toward increasing ion acoustic wave intensities with decreasing solar wind velocity.

compression zone ahead of the high-speed stream (see, for example, *Hundhausen* [1972]), is clearly evident in Figures 4 and 6. As can be seen in Figure 4, several periods of sporadic ion acoustic wave activity are evident for nearly 3 days before the onset of the high-speed stream. These waves reach their highest intensities from about 1200 to 2400 UT on day 73, about 16 hours ahead of the stream interface. A few sporadic bursts of ion acoustic waves are also evident from about 0940 to 1130 UT on day 74, immediately after the stream interface but before the proton flow speed has reached its maximum value. Electron plasma oscillations are also evident in this same region.

3. Correlation With T_e/T_p

A well-known characteristic of the ion acoustic mode is that the damping, and hence stability, of this mode is strongly influenced by the electron to ion temperature ratio T_e/T_i [*Stix*, 1962]. For values of T_e/T_i less than 1, the phase velocity of the ion acoustic mode is comparable to the thermal velocity of the ions, and the wave is strongly damped by Landau damping. As T_e/T_i increases above 1, the phase velocity increases, and the number of resonant ions, and hence the damping, rapidly decreases. The ion acoustic mode is therefore difficult to drive

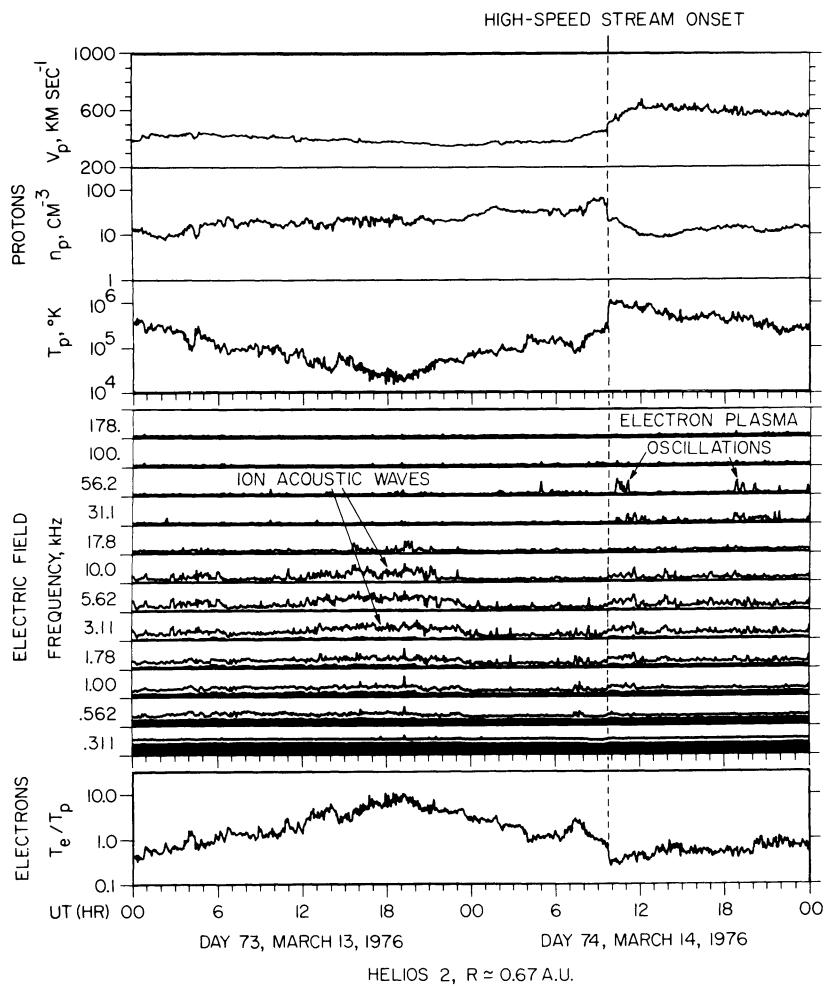

Fig. 6. Details of the plasma wave electric field intensities and solar wind plasma parameters for the high-speed solar wind stream onset on day 74, 1976, from Figure 4. The largest ion acoustic wave intensities during this period occur in the region of large T_e/T_p immediately preceding the high-speed stream onset.

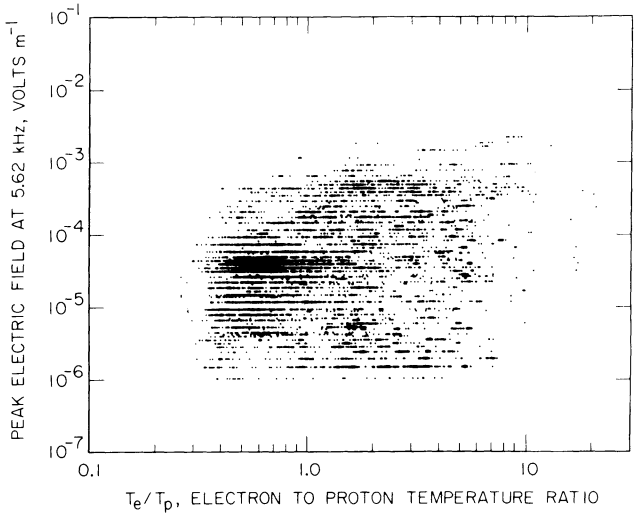

Fig. 7. A scatter plot of the ion acoustic wave electric field intensities as a function of T_e/T_p for the three solar rotations shown in Figures 2, 3, and 4. Although a considerable amount of scatter exists in these data, the general trend toward increasing electric field intensity with increasing T_e/T_p is clearly evident.

unstable for values of T_e/T_i less than or comparable to 1. Because the electrostatic waves under consideration are thought to be caused by an ion acoustic instability, it is of considerable interest to investigate the relationship between the intensity of these waves and the corresponding electron to ion temperature ratios.

Because of the non-Maxwellian anisotropic character of the solar wind plasma, several different methods can be used to compute the electron and proton temperatures. For this study, all temperatures have been computed from the second moment of the velocity distribution function $f(\mathbf{V})$:

$$nk\mathbf{T} = \tfrac{1}{2}m\int f(\mathbf{V})(\mathbf{V} - \mathbf{U})^2\, d^3V$$

where k is Boltzmann's constant, m is the particle mass, and U is the bulk velocity. Since the solar wind ion acoustic waves are known to be propagating approximately parallel to the magnetic field, ideally one should use the temperature parallel to the magnetic field. However, since the angular field of view of the electron instrument is restricted to a 18° wide disk in the ecliptic plane, it is not possible to measure parallel electron temperatures if the magnetic field is more than about ±10° from the ecliptic plane. To provide the best estimate of the parallel temperature, the electron temperature has been computed along a direction parallel to the projection of the magnetic field in the ecliptic plane. The proton temperature has been computed along the spacecraft-sun line. Comparison with the temperature tensor resulting from a complete analysis of the three-dimensional proton measurements shows reasonable agreement provided the **B** vector is within a 45° cone around the radial direction. In addition, since the temperature anisotropies are normally less than a factor of 2, the errors introduced by this simplified analysis are not expected to be large. In any case, these temperatures are considered adequate for this initial survey. More detailed analyses of the electron and proton distribution functions for a specific case are presented later.

As can be seen from the T_e/T_p plots in Figures 2, 3, and 4, the temperature ratio varies considerably during any given solar rotation, from about 0.5 to greater than 10. These variations are mainly due to changes in the proton temperature, since the electron temperature tends to remain relatively constant at about (1–2) × 10^5 °K. Comparisons of the T_e/T_p variations with the ion acoustic wave intensities generally show a good correlation, with a strong tendency for the wave intensities to be large when T_e/T_p is large. For example, the large increases in T_e/T_p centered on days 326, 331, and 341 in Figure 2, on days 357, 2, and 10 in Figure 3, and on days 73, 82, and 88 in Figure 4 are all associated with periods of enhanced ion acoustic wave activity. The correlation with T_e/T_p can be seen in further detail in Figure 6, which shows that the intense burst of ion acoustic waves from about 1200 to 2400 UT on day 73 is centered on a region of unusually large T_e/T_p, with $T_e/T_p \simeq 10$ at 1900 UT.

The correlation between the ion acoustic wave intensities and T_e/T_p is presented on a more quantitative basis by the scatter plot in Figure 7. This illustration shows the peak electric field intensities at 5.62 kHz, approximately in the center of the ion acoustic wave spectrum, and the corresponding T_e/T_p values for all of the data in Figures 2, 3, and 4. Although a fair amount of scatter exists, the general trend toward larger electric field intensities at larger values of T_e/T_p is clearly evident. This correlation can be demonstrated even more clearly if the peak electric field intensities are averaged and plotted as a function of T_e/T_p, as is shown in Figure 8. As can be seen, the average ion acoustic wave intensities increase by about a factor of 7, from 70 to 500 μV m^{-1}, as the electron to proton temperature ratio increases from 1.0 to 10.

The T_e/T_p correlation described above also fits in well with the overall morphology of the ion acoustic wave activity and the relationship to the high-speed stream structure discussed in the preceding section. A well-established observational feature of the solar wind plasma flow is that the proton temperature tends to be largest in the high-speed streams and drops substantially in the low-speed regions [*Hundhausen*, 1972]. Sometimes the proton temperature in the region immediately ahead of the high-speed stream drops to extremely low values, ~10^4 °K, as is illustrated by the example in Figure 6. Since the electron temperature does not change by very much across the stream interface, this pattern usually results in large T_e/T_p values ahead of the high-speed stream interface, in the region where the ion acoustic waves tend to be most intense.

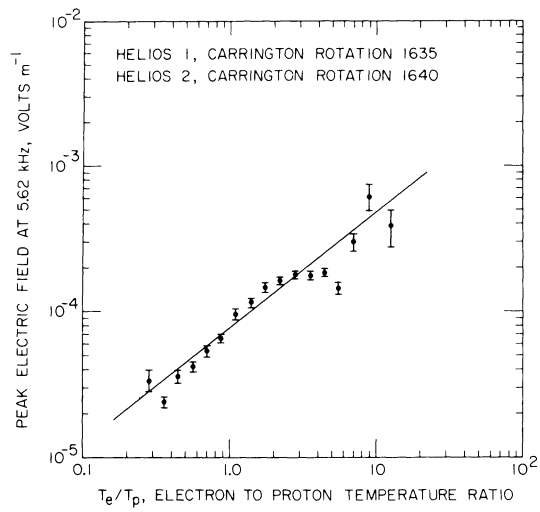

Fig. 8. A further detailed analysis of the data in Figure 7, showing the average of the 36-min peak electric field intensities as a function of T_e/T_p. The error bars give the standard deviation of the average T_e/T_p in each interval. The ion acoustic wave intensity increases by about a factor of 7 as T_e/T_p increases from 1 to 10.

Overall, the observed correlation of the electrostatic wave intensities with T_e/T_p supports the view that these waves are an ion-acoustic-like mode. One unexplained feature of this correlation is the fact that although the electric field intensities tend to increase as T_e/T_p increases, substantial ion acoustic wave intensities sometimes occur even when T_e/T_p is quite small. For example, in Figure 6 a moderately intense burst of ion acoustic waves can be seen from about 0930 to 1130 UT on day 74, in a region where T_e/T_p is approximately 0.3. Since the ion acoustic mode should be strongly damped under these conditions, an important question arises as to how the ion acoustic mode can be unstable in regions such as this and what feature of the proton and electron velocity distribution is responsible for the instability. The presence of electron plasma oscillations in this same region suggests that some unusual suprathermal particle distributions are probably present immediately following the high-speed stream interface which may also be responsible for generating these waves.

4. Comparisons With Electron and Proton Distribution Functions and Related Parameters

Since the generation of the solar wind ion acoustic waves must involve some suitable source of free energy, detailed comparisons have been made with the electron and proton distribution functions to try to identify the primary feature of the distribution function which is responsible for these waves. A typical example of these comparisons is illustrated by the electron distribution function in Figure 9. This distribution function was selected from the period of very intense ion acoustic wave activity in Figure 6.

The top panel of Figure 9 shows a contour diagram of the electron distribution function at about 1702:50 UT on day 73, near the time of maximum wave intensity. The electron distribution functions are measured by using a detector viewing radially outward from the spacecraft spin axis. The spin axis is oriented perpendicular to the ecliptic plane. The contour diagram in the top panel of Figure 9 therefore represents a cut through the distribution function parallel to the ecliptic plane. To assure that all possible pitch angles with respect to the magnetic field are contained within such a cut, the measurement in Figure 9 was selected at a time when the magnetic field direction was nearly parallel, $\theta_B = -9.8°$, to the ecliptic plane. The magnetic field direction projected onto the ecliptic plane is indicated by the dashed line in the top panel of Figure 9. A one-dimensional cross section of the electron distribution function along the direction of the magnetic field, with positive velocities away from the sun, is shown in the bottom panel of Figure 9. The best fit Maxwellian distribution function for the core electrons is also indicated in Figure 9. The core temperature, parallel to the magnetic field, in this case is $T_{\parallel} = 1.4 \times 10^5$ °K. A detailed description of the methods used to compute these distribution functions will be given elsewhere.

As can be seen from Figure 9, the electron distribution function is a monotonically decreasing function of velocity in all directions with respect to the magnetic field and shows no evidence of a double peak in the distribution function over the entire energy range, 10 eV to 1.6 keV, for which measurements are available. Measurements at even higher energies, >20 keV, (E. Keppler, personal communication, 1978) also show no evidence of a double peak. The only identifiable feature of the distribution function which could contribute to the free energy available for generating waves is the slight asymmetry, parallel and antiparallel to the magnetic field, caused by the electron heat flux. The computed heat flux in this case is $Q_e = 2.2 \times 10^{-2}$ erg cm^{-2} s^{-1}. The relative drift induced between the core electrons and the solar wind protons by this heat flux has been suggested by *Forslund* [1970] as a possible mechanism for producing ion acoustic waves in the solar wind.

To provide an overall evaluation of the possible role of the electron heat flux as the source of the interplanetary ion acoustic waves, the electron heat flux has been plotted in the bottom panels of Figures 2, 3, and 4. Whenever possible, the electron parameters were computed when the magnetic field was within ±10° from the ecliptic plane. Large variations in the electron heat flux are clearly evident, even on relatively short time scales. Detailed comparisons with the ion acoustic wave intensities show that the heat flux is usually relatively large, 10^{-2} to 10^{-1} erg cm^{-2} s^{-1}, in the region where the ion acoustic waves occur. This relationship is illustrated in better detail by the scatter diagram in Figure 10, which shows the electric field intensity at 5.62 kHz as a function of electron heat flux Q_e for the three solar rotations in Figures 2, 3, and 4. As can be seen, the electric field intensities show a very clear correlation with Q_e, increasing in intensity with increasing heat flux. Since the physically relevant parameter for the electrostatic heat flux instability is the skewness of the electron velocity distribution

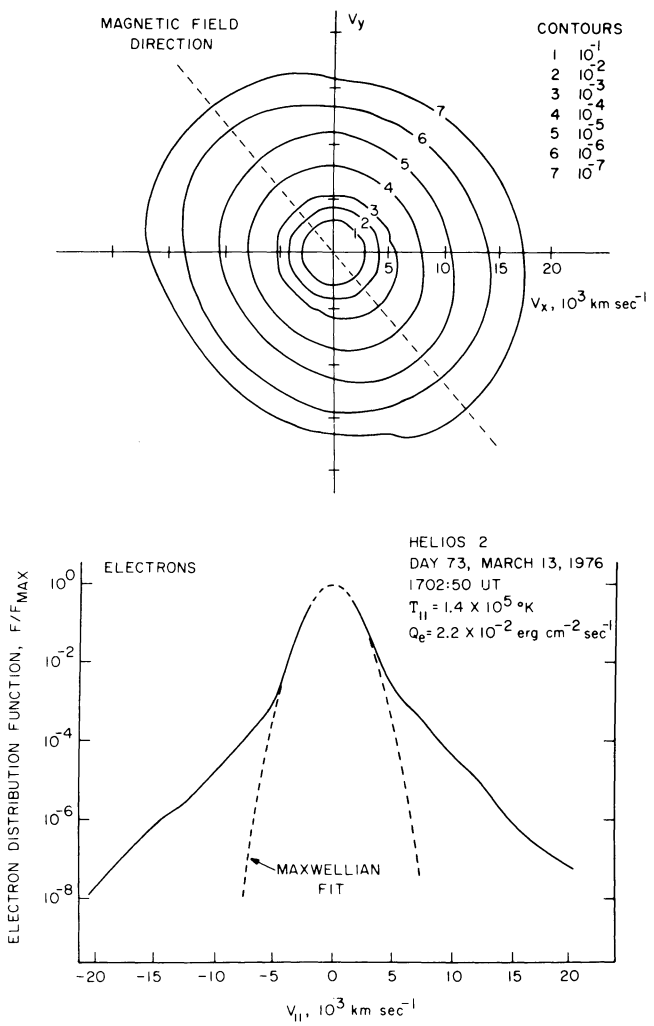

Fig. 9. The electron distribution function for the period of intense ion acoustic wave activity in Figure 6 at about 1702:50 UT on day 73. The only source of free energy evident in the electron velocity distribution which could drive the ion acoustic waves is the asymmetry due to the electron heat flux.

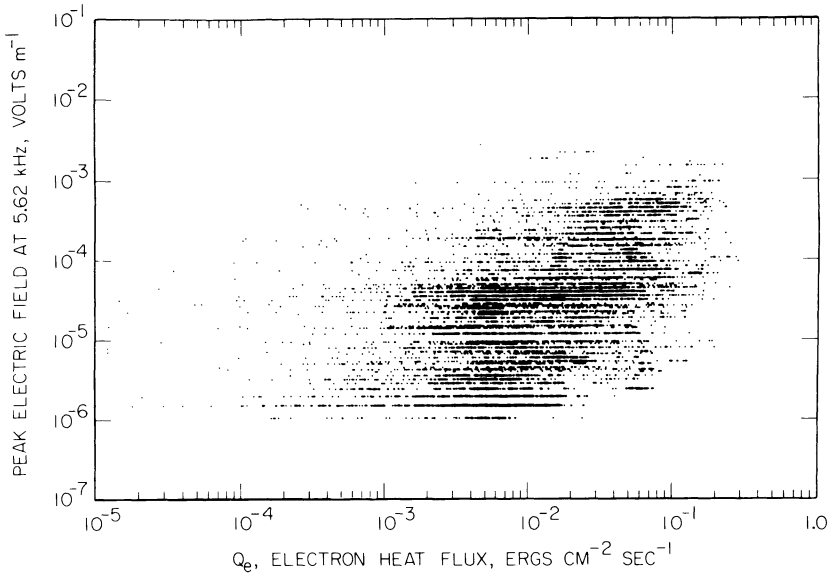

Fig. 10. A scatter plot of the ion acoustic wave electric field intensities as a function of the electron heat flux for the three solar rotations shown in Figures 2, 3, and 4. The electric field intensity shows a clear correlation with the heat flux, increasing with increasing Q_e.

function [*Forslund,* 1970; *Gary,* 1978*b*], the average electric field intensities have also been computed as a function of the normalized electron heat flux, $Q_e/n_e m_e V_{th}^3$, where V_{th} is the core electron thermal velocity. The results of this analysis are illustrated in Figure 11, which shows a rapid increase in the electric field intensities as the normalized electron heat flux increases. Of particular interest is the rapid increase in the electric field strength when the normalized heat flux exceeds about 0.1, which suggests an approximate threshold condition for the ion acoustic instability.

To investigate the possible relationship with the solar wind proton distributions, Figure 12 shows a representative proton distribution function selected from a period of intense ion acoustic wave activity. This distribution function is from about 1700:08 UT on day 73, nearly simultaneous with the electron distribution function in Figure 9. Since the plasma instruments on Helios measure the full three-dimensional distribution function of the solar wind protons, cuts and projections of the proton distribution function can be made in any desired plane. The top panel of Figure 12 shows a cross section of the proton distribution function in a plane containing the magnetic field and the spacecraft-sun line. The positive V_x axis is directed toward the sun, and the magnetic field direction is indicated by the dashed line. The bottom panel shows the reduced one-dimensional distribution function $F(V)$ obtained by integrating over velocities perpendicular to the magnetic field. Details of the procedures used to compute these distribution functions are given by *Marsch et al.* [1979].

As can be seen from Figure 12, the proton distribution function in the region where the intense ion acoustic waves are observed displays a marked asymmetry with respect to velocities parallel and antiparallel to the magnetic field. This asymmetry is caused by the presence of a double-proton stream of the type discussed by *Feldman et al.* [1973*a*, *b*] and *Rosenbauer et al.* [1977]. The secondary proton stream in this case has a velocity shift of about 80 km s^{-1} with respect to the main solar wind stream and a relative density of about 3%. Although the shoulder on the distribution function is caused by the secondary stream, the distribution function does not have a clearly resolved double peak, at least not within the velocity resolution of the instrument, which is about 30 km s^{-1}.

The fact that a double-proton stream is present in the region of intense ion acoustic waves is of considerable interest, since *Gary* [1978*a*] has proposed that these waves are caused by an 'ion-acoustic-like' instability driven by a double-ion beam. Whether or not the double-proton stream in Figure 12 can actually produce this instability is a question which will be discussed later. Observationally, detailed inspection of the proton distribution function for cases in which ion acoustic waves are present nearly always shows some evidence of a double-proton stream. However, in most cases the secondary proton stream is not resolved into a separate peak, but rather appears as a shoulder on the main proton distribution, as in Figure 12.

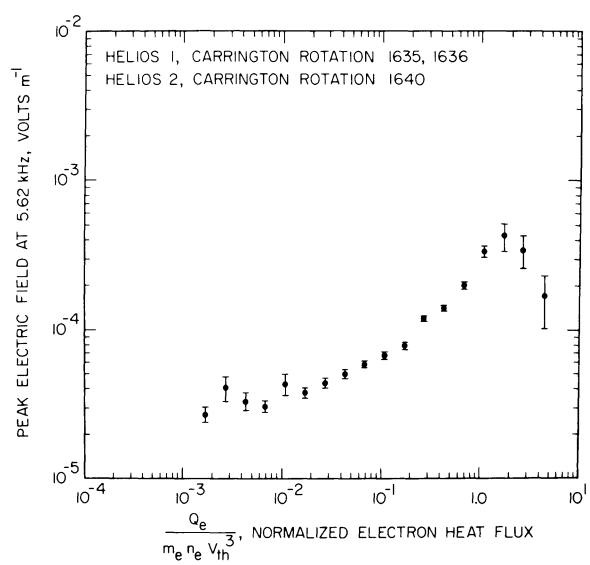

Fig. 11. The average of the peak 36-min electric field intensities as a function of the normalized electron heat flux, $Q_e/n_e m_e V_{th}^3$, where V_{th} is the electron thermal velocity. The error bars give the standard deviation of the average electron heat flux in each interval.

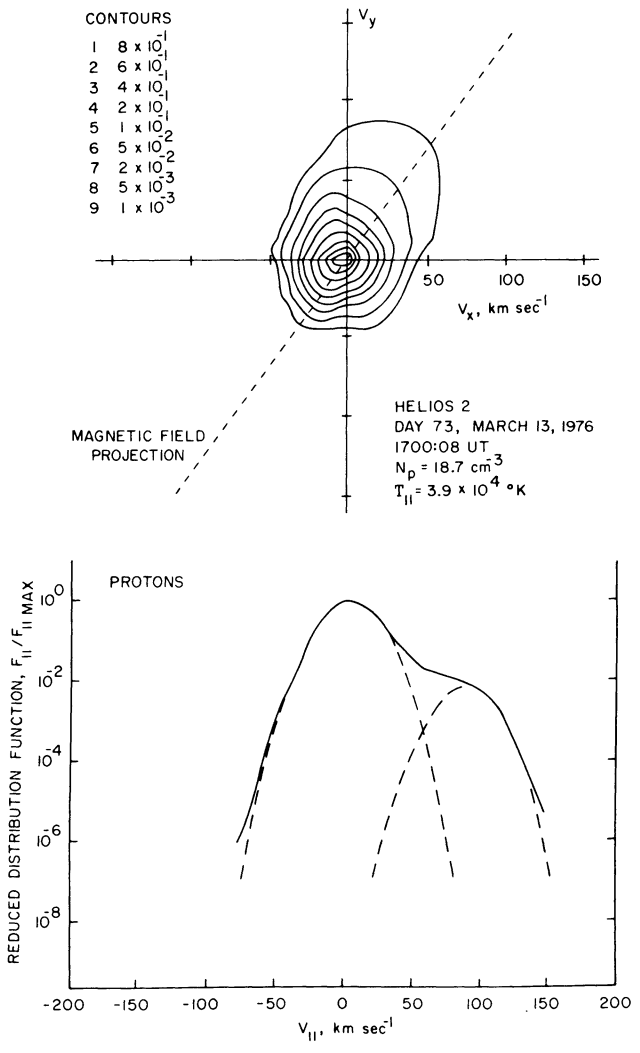

Fig. 12. The proton distribution function for the period of intense ion acoustic waves in Figure 6 at about 1700:08 on day 73, very close to the time for the electron spectrum in Figure 9. The large asymmetry in the reduced one-dimensional distribution function is caused by a double-proton stream. Double-proton streams of this type, usually consisting of a broad shoulder on the main solar wind proton distribution, are usually present in the regions where the ion acoustic waves are observed.

At the present time it is difficult to put the correlation with double-proton streams on a clear quantitative basis, since it is very time consuming and costly to compute individual stream parameters from the three-dimensional measurements for a large quantity of data, such as would be required for a detailed statistical analysis. To provide a rough quantitative indication of the level of correlation, we have compared the ion acoustic wave intensities with the one-dimensional fit parameter χ^2, which indicates how well the radial proton flux fits a Maxwellian velocity distribution. The main utility of the χ^2 parameter is that it is readily available for all of the plasma data and that any deviation from a simple Maxwellian, such as one due to a double-proton stream, is indicated by an increase in χ^2. The main disadvantages are that the fit parameter does not detect deviations from a Maxwellian in directions transverse to the radial direction and that other types of deviations, not attributable to double-proton streams, can affect χ^2. Practically, although a large χ^2 does not uniquely identify the presence of a double-proton stream, our experience from investigating individual cases is that a large χ^2, $\gtrsim 100$, provides a reasonably reliable indication of a double-proton stream. A plot of the average 5.62-kHz electric field intensities as a function of χ^2 is shown in Figure 13, using all of the available data. As can be seen, the electric field intensities show a moderately good correlation with χ^2, thereby indicating that double-proton streams are usually present when the ion acoustic wave intensities are large. The correlation of the ion acoustic wave intensities with double-proton streams also fits in well with the overall morphology of the ion acoustic wave activity, since, as is discussed by *Feldman et al.* [1973*b*], double-ion streams tend to occur in the low-velocity regions between high-speed streams, which is where the ion acoustic wave intensities are usually the largest. Although a correlation with double-proton streams clearly exists, it is still by no means certain that double-proton streams provide the free energy to generate the ion acoustic waves, since the double-peaked proton distribution required for the ion beam instability is usually not observed.

5. Summary and Discussion

In this paper we have investigated the relationship of interplanetary ion acoustic waves to the large-scale corotational structure of the solar wind and to various detailed plasma parameters. The results of this study show that the ion acoustic waves usually occur with the greatest intensity and frequency of occurrence in the low-speed regions immediately preceding the onset of a high-speed stream. Comparisons with the detailed plasma parameters show that the ion acoustic waves have a good correlation with the electron to proton temperature ratio, increasing in intensity by about a factor of 7 as the electron to proton temperature ratio increases from 1.0 to 10.0. The electron velocity distribution functions in the region where the ion acoustic waves occur are usually monotonic over a large range of energies and do not show any evidence of a double peak which could drive an electrostatic instability. The only source of free energy which can be identified in the

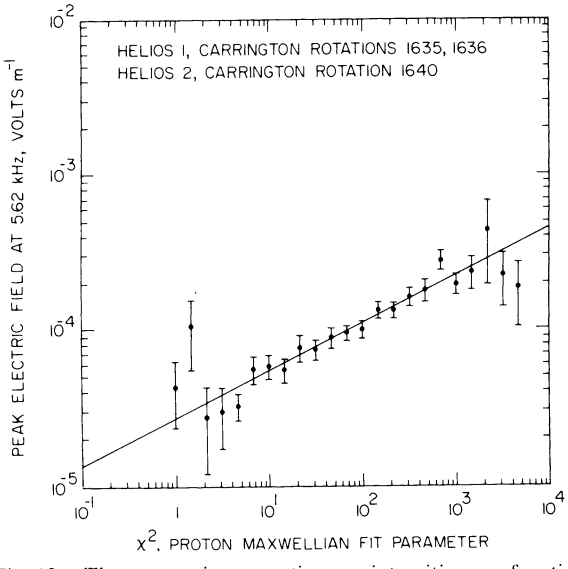

Fig. 13. The average ion acoustic wave intensities as a function of the Maxwellian fit parameter χ^2 for all of the available Helios 1 and 2 data. Large values of χ^2 indicate large deviations of the proton distribution from a Maxwellian, such as occur when a double-proton stream is present. The positive correlation between χ^2 and the ion acoustic wave intensities indicates that the ion acoustic waves tend to occur in regions where a double-proton stream is present.

electron velocity distribution function is the asymmetry caused by the electron heat flux. Detailed comparisons show that the ion acoustic wave intensities have a good correlation with the electron heat flux, increasing by about a factor of 10 as the normalized heat flux increases from 0.1 to greater than 1.0. The only source of free energy that can be identified in the proton distribution function is the occurrence of double-proton streams. Examination of the proton distribution function in the regions where the ion acoustic waves are observed usually shows evidence of a double-proton stream. Detailed statistical analyses also show a good correlation with the χ^2 parameter, which indicates the presence of a double-proton stream. The secondary proton stream is, however, almost never clearly resolved into a separate peak, but rather appears as a shoulder on the main solar wind proton distribution.

Although an extensive study has been undertaken to try to identify the primary features of the plasma distribution responsible for the solar wind ion acoustic waves, it has become increasingly clear that a combination of parameters controls the generation of these waves and that at the present time a definitive identification of the instability mechanism is probably not possible. One inherent problem is that because of the complex interdependence of the various solar wind parameters, it is very difficult with a statistical analysis to identify conclusively the relevant parameters that control the generation of these waves. Nonetheless, the results of this study do provide important limitations on the possible instability mechanisms and provide a quantitative basis for further theoretical analysis.

When the possible mechanisms for generating the ion acoustic waves are considered, there appear at the present time to be three general possibilities: (1) the waves are ion acoustic waves driven by the electron heat flux, as has been suggested by *Forslund* [1970]; (2) the waves are an ion-acoustic-like mode driven by a double-proton stream, as was suggested by *Gary* [1978*a*]; or (3) the waves are driven by a yet undetected feature of the velocity distribution function. The favorable and unfavorable features associated with each of these possibilities are now considered in detail.

The good correlation of the ion acoustic wave intensities with the electron heat flux and with T_e/T_p provides substantial support for the suggestion of *Forslund* [1970] that ion acoustic waves could be driven unstable in the solar wind by the electron heat flux. As was pointed out by *Gary* [1978*a*], the principal difficulty with the electron heat flux mechanism is that for typical values of T_e/T_p the relative drift velocity induced between the core electrons and the solar wind protons is too small to drive the ion acoustic instability. If we take favorable cases, such as the case in Figure 6 at about 1800 UT, where $T_e/T_p \simeq 10$, then it can be demonstrated that the ion acoustic mode is very close to instability. For example, by using the measured electron heat flux Q_e, the relative drift velocity v_{0c} between the core electrons and the solar wind protons can be estimated by using equation (4) of *Feldman et al.* [1975]:

$$Q_e = \frac{5}{2} n v_{0c} k T_e \left(\frac{T_h}{T_c} - 1 \right) \tag{1}$$

where T_c and T_h are the electron core and halo temperature and k is the Boltzmann constant. Using the measured values of $Q_e = 2.2 \times 10^{-2}$ erg cm^{-2} s^{-1}, $T_c = 1.4 \times 10^5$ °K, and $T_h = 8.4 \times 10^5$ °K, (1) above gives $v_{0c} = 47$ km s^{-1}. Using the measured electron temperature of $T_e = 1.4 \times 10^5$ °K, the ratio of the relative drift velocity to the electron thermal speed is $v_{0c}/v_{th} = 3.2 \times 10^{-2}$. Using the plot of the critical drift velocity for electrostatic instability given by *Freid and Gould* [1961] and $T_e/T_i = 10$, it can be shown that the drift velocity is close to instability, within about a factor of 2. Thus in this case the electron heat flux mechanism provides a reasonable explanation for the observed.

However, in other cases, such as can be seen in Figure 6, ion acoustic waves with substantial intensities are still present when $T_e/T_p \simeq 1$. The observations of ion-acoustic-like waves at such low values of T_e/T_p represent a serious problem for the electron heat flux mechanism. Nonetheless, various possibilities exist for improving this situation which need to be further explored. For example, the proton temperatures in this study are a best fit to the entire proton distribution, including any double-proton stream contribution, and are therefore somewhat too large for purposes of computing the ion acoustic instability thresholds. Also, deviations of the proton distribution from a Maxwellian may occur in such a way as to reduce the proton Landau damping. Further consideration of these effects involves very detailed computer analyses using the measured distribution functions and will be discussed in a future paper [*Dum et al.*, 1979].

The frequent observation of double-proton streams in association with the solar wind ion acoustic waves also gives substantial support for the proposal of *Gary* [1978*a*] that these waves are produced by an electrostatic double-ion beam instability. However, detailed modeling calculations using the observed proton distribution functions show that it is difficult to satisfy the instability criterion for the ion beam mode. The basic reason for this difficulty is that the double-proton streams usually are not well enough resolved to produce a two-stream instability. Typically, the proton beam only appears as a shoulder on the main proton distribution as in Figure 12. The absence of a clearly defined double peak probably cannot by itself be taken as evidence against this mechanism, since the instrument resolution of about 30 km s^{-1} may in some cases smear out the minimum between the two peaks. Also, wave-particle interactions may act to fill in the minimum in such a way as to produce a marginally stable distribution. If we ignore the fact that the minimum usually does not exist and try to fit observed proton distributions to two Maxwellians, some rough comparisons can be made with Gary's instability threshold calculations. For example, the two Maxwellian distributions indicated by the dashed lines in Figure 10 give a ratio of the beam density to the main stream density of $n_b/n_m = 0.03$, a ratio of the beam temperature to the main stream temperature of $T_b/T_m = 1.1$, a ratio of the electron temperature to the main proton stream temperature of $T_e/T_m = 6.67$, and a ratio of the beam velocity to the main stream thermal velocity of $V_0/V_m = 3.0$. Comparison of these parameters with the ion beam instability calculations in Figure 4 of *Gary* [1978*a*] shows that the ion beam mode should be stable for these conditions. These results are in agreement with the recent comparisons of *Lemons et al.* [1979], in which it was also concluded that the ion beam mode is stable, although not by a large factor. The main advantage of the ion beam instability in comparison to the electron heat flux instability is that for a given T_e/T_p the ion beam instability can occur at a lower relative drift speed between the core electrons and the main proton stream. In this sense, the ion beam mode seems to offer the best possibility for explaining the existence of these waves, although the detailed reasons for the discrepancy in the instability threshold are not understood. Many possible explanations for the observed discrepancies can be offered, including, for example, the occurrence of small-scale spatial irregularities in the proton distribu-

tion function which cannot be resolved or large velocity space irregularities in the beam which cannot be detected by the plasma analyzer.

Because of the uncertainties in establishing the mechanism responsible for the interplanetary ion acoustic waves, other possible sources of free energy should be mentioned which could possibly be responsible for these waves. One possible nonthermal effect which could have escaped observation by Helios is the low-energy ($5 \lesssim E \lesssim 50$ keV) protons observed by *Frank* [1970] in the interplanetary medium. These suprathermal proton streams occur sporadically for periods of a few days every few weeks, with a frequency of occurrence comparable to the solar wind ion acoustic waves. The possibility that such proton streams could cause the interplanetary ion acoustic waves is also supported by the fact that somewhat similar proton streams from the earth's bow shock, although of higher intensity, are known to produce waves similar to the ion acoustic waves detected by Helios far from the earth [*Gurnett and Frank*, 1978]. Waves of this type have also been observed by Voyager in association with interplanetary shocks [*Kurth et al.*, 1979]. Since Helios does not have instrumentation suitable for detecting protons in this energy range ($5 \lesssim E \lesssim 50$ keV), nothing is currently known about the possible association of the ion acoustic waves with these low-energy proton streams.

In conclusion, the results of this study provide support for both the electron heat flux and the double-ion beam mechanisms for generating the solar wind ion acoustic waves, although each mechanism has problems under certain conditions, particularly for low values of T_e/T_p. The positive correlation with T_e/T_p and the electron heat flux is expected for both the electron heat flux and double-ion mechanisms. The main difficulty with the double-ion beam mechanism is that the proton distributions usually do not have the clearly resolved double peak required for instability. This difficulty could be the result of insufficient velocity or spatial resolution to resolve the two peaks. It is also possible that more than one mechanism could be operative in the solar wind to produce these waves. From the electric field measurements alone it is impossible to distinguish between the various mechanisms which can produce electrostatic waves propagating parallel to the magnetic field with wavelengths near $2\pi\lambda_D$, since the large Doppler shifts essentially destroy all information on the frequency spectrum in the rest frame of the plasma. It is hoped that in the future, more detailed studies of the plasma distribution functions, and their implications with regard to the various instability mechanisms, will provide a definitive determination of the plasma instability mechanism responsible for these waves.

Acknowledgments. The authors would like to express their appreciation to C. Dum and P. Gary for their helpful comments and suggestions during the preparation of this manuscript and to R. Anderson, K. Muhlhauser, and G. Voots for their assistance in the data analysis. We also thank F. Neubauer from the Technischen Universitat Braunschweig for providing the magnetic field data used in this study. The research at the University of Iowa was supported by NASA under contract NAS5-11279 and grant NGL-16-001-043. The research at the Max-Planck-Institut was supported by the Deutsches Bundeministerium für Forschung und Technologie.

The Editor thanks R. W. Fredricks and D. S. Lemons for their assistance in evaluating this paper.

REFERENCES

Buneman, O., Instability, turbulence and conductivity in a current-carrying plasma, *Phys. Rev. Lett., 1,* 8, 1958.

Dum, C. T., E. Marsch, W. Pilipp, and D. A. Gurnett, Ion sound turbulence in the solar wind, in *Solar Wind 4,* Springer, New York, in press, 1979.

Feldman, W. C., J. R. Asbridge, S. J. Bame, and M. D. Montgomery, Double ion streams in the solar wind, *J. Geophys. Res., 78,* 2017, 1973*a*.

Feldman, W. C., J. R. Asbridge, S. J. Bame, and M. D. Montgomery, On the origin of solar wind proton thermal anisotropy, *J. Geophys. Res., 78,* 6451, 1973*b*.

Feldman, W. C., J. R. Asbridge, S. J. Bame, M. D. Montgomery, and S. P. Gary, Solar wind electrons, *J. Geophys. Res., 80,* 4181, 1975.

Forslund, D. W., Instabilities associated with the heat conduction in the solar wind and their consequences, *J. Geophys. Res., 75,* 17, 1970.

Frank, L. A., On the presence of low-energy protons ($5 \lesssim E \lesssim 50$ keV) in the interplanetary medium, *J. Geophys. Res., 75,* 707, 1970.

Freid, B. D., and R. W. Gould, Longitudinal ion oscillations in a hot plasma, *Phys. Fluids, 4,* 139, 1961.

Gary, S. P., Ion-acoustic-like instabilities in the solar wind, *J. Geophys. Res., 83,* 2504, 1978*a*.

Gary, S. P., Electrostatic heat flux instabilities, *J. Plasma Phys., 20,* 47, 1978*b*.

Gosling, J. T., J. R. Asbridge, S. J. Bame, and W. C. Feldman, Solar wind interfaces, *J. Geophys. Res., 71,* 1401, 1978.

Gurnett, D. A., and R. R. Anderson, Plasma wave electric fields in the solar wind: Initial results from Helios 1, *J. Geophys. Res., 82,* 632, 1977.

Gurnett, D. A., and L. A. Frank, Ion acoustic waves in the solar wind, *J. Geophys. Res., 83,* 58, 1978.

Hundhausen, A. J., *Coronal Expansion and Solar Wind,* Springer, New York, 1972.

Kurth, W. S., D. A. Gurnett, and F. L. Scarf, High-resolution spectrograms of ion acoustic waves in the solar wind, *J. Geophys. Res., 84,* in press, 1979.

Lemons, D. S., J. R. Asbridge, S. J. Bame, W. C. Feldman, S. P. Gary, and J. T. Gosling, The source of electrostatic fluctuations in the solar wind, *J. Geophys. Res., 84,* this issue, 1979.

Marsch, E., W. Pilipp, H. Rosenbauer, R. Schwenn, K.-H. Mühlhäuser, Characteristics of the three-dimensional proton distribution in the solar wind observed by Helios between 0.3 and 1 AU, in *Solar Wind 4,* Springer, New York, in press, 1979.

Rosenbauer, H., R. Schwenn, E. Marsch, B. Meyer, H. Miggenrieder, M. D. Montgomery, K. H. Mühlhäuser, W. Pilipp, W. Voges, and S. M. Zink, A survey on initial results of the Helios plasma experiment, *Z. Geophys., 42,* 561, 1977.

Schwenn, R., H. Rosenbauer, and H. Miggenrieder, Das Plasmaexperiment auf Helios (E1), *Raumfahrtforschung, 19*(5), 226, 1975.

Stix, T. H., *The Theory of Plasma Waves,* McGraw-Hill, New York, 1962.

(Received October 19, 1978;
revised January 4, 1979;
accepted January 4, 1979.)